Influence of outer medium viscosity on the motion of rolling droplets down an incline

Muhammad Rizwanur Rahman and Prashant R. Waghmare*
interfacial Science and Surface Engineering Lab (iSSELab), Department of Mechanical Engineering, University of Alberta, Edmonton, Alberta T6G2G8, Canada

(Received 4 August 2017; published 2 February 2018)

The role of medium viscosity on a non-deformable rolling body has long been understood while its deformable counterpart still awaits clarification. In this article, we present a scaling analysis with experimental evidences to demonstrate that in creeping flow, medium viscosity significantly alters how the descent speed of a drop responds to an increase in drop size. While descending down an incline in a viscous medium, a rolling drop may travel with either increasing or decreasing velocities as its size increases. The boundary between these two motion behaviors can be maneuvered by altering the viscosity of the surrounding medium.

DOI: 10.1103/PhysRevFluids.3.023601

I. INTRODUCTION

In the study of deformable body motion in a viscous medium, the dynamics become complicated due to dissipation from fluid motion inside and outside the body. In contrast to the case of a rolling non-deforming sphere, shape deformation, interfacial interactions (interfacial tensions and/or wettability) as well as contact line dissipation cannot be ignored in case of a rolling deformable body, such as a liquid drop. With recent advancements in micro-fluidics and an upsurge in the use of micro/nano-fabrication techniques for numerous applications [1–3], the motion of droplets on solid surfaces in viscous media demands a thorough understanding. For example, it remains debatable [4] whether a liquid drop rolls or slides along a solid surface, particularly for low-energy surfaces with very low roll-off angle. A defined criterion that demarcates these two types of motion is difficult to establish; in fact, an overlap between them has been witnessed during the transition from rolling to sliding motion [5,6]. Mahadevan and Pomeau [7] discovered that, unlike solid spheres, the velocity of a rolling liquid drop in air varies inversely with drop size. In this case, viscous dissipation at the contact area constitutes a form of resistance that varies based on the drop radius. This results in the inverse relation between drop size and its traveling velocity. For small droplets, inertia and viscous dissipation compete to dictate the outcome and in most cases the latter dominates the physics of the flow [7]. Richard and Quéré [4] experimentally verified this claim provided the drops maintain quasi-static shape [7,8].

While the importance of medium viscosity is well established for cases of solid-body motion [9–14], the role of the medium viscosity is ignored in most of the deformable-body motion experiments. Griggs *et al.* [15,16] numerically and experimentally studied the motion of deformable drops sliding on an incline and paid particular attention to the role of the viscous medium. The authors discussed the possibility of the existence of two speed regimes. However, in most of the cases they analyzed, the drop size was beyond the capillary length scale limit resulting in sliding motion. Experimental evidence of the two rolling regimes, supported by a unified scaling argument, is still missing from the literature.

*Corresponding author: waghmare@ualberta.ca

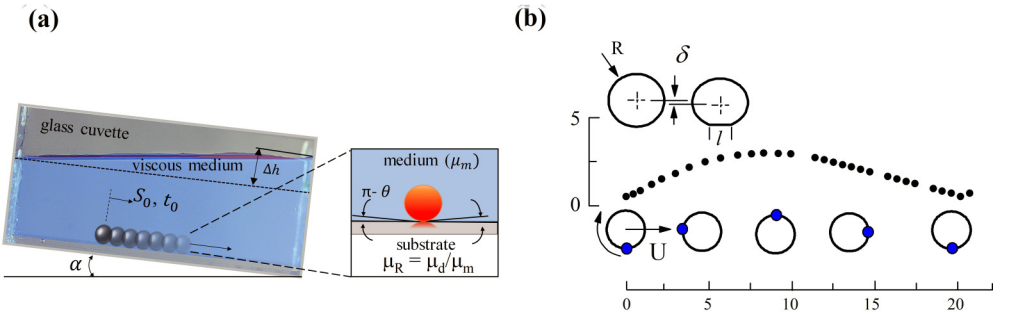

FIG. 1. (a) Schematic of the experimental setup for observing the droplet motion along an inclined plane (not to scale). Snapshots of the moving droplet along its trajectory parallel to the bottom plane of the cuvette are provided, which were used to perform our analysis. The effect of the difference in the liquid reservoir level, denoted as Δh, is ignored in this analysis. The inset shows the instantaneous contact angle (θ) of the drop during its motion. The observed motion is assumed to be a rolling motion for very low contact angle hysteresis ($\Delta\theta \leqslant 7^\circ$) and high contact angle of the non-wetting drop [4]. (b) The lowering of the drop's center of mass due to its weight has been denoted by δ as shown in the schematic [7]. As a drop moves forward, we tracked a small marker on the drop which exhibits cycloidal trajectory. The schematic presented below the experimental data further depicts the motion of the marker as the drop rolls; the linear motion of the center of mass of the drop is denoted by U, the straight arrow indicates the direction of this velocity (U) and the curved arrow shows the direction of the droplet's rotation.

In order to fill this gap in the literature, we turned our attention to the role of the surrounding medium viscosity on the motion of liquid droplets on an incline. This exercise allows us to observe two distinct regimes (we will denote these two regimes as Regimes I and II) for size-dependent velocity and comment on the parameters that demarcate the two speed regimes and therefore identifying the boundary between them. While our experimentation with single phase liquid drops confirms Regime I behavior and supports the scaling model developed in this study, the exploration of Regime II required us to alter the experimental domain by using a double emulsion drop to overcome the difficulties associated with a single phase drop rolling in this regime.

II. EXPERIMENTAL METHODS

The experiment included the deposition of a drop on a glass substrate immersed in a viscous medium using a needleless deposition technique [17]. A schematic of the experimental setup is shown in Fig. 1(a). Droplet motion was triggered by precisely inclining the arrangement to an inclination angle (α). The drop's trajectory—from the deposited location to a point well beyond the position where it has reached terminal velocity—was recorded for further analysis. Since needleless drop deposition is a substrate independent method, we can avoid any unwarranted effects such as deformation of the droplet during deposition [17–19].

To investigate the role of medium viscosity on the drop trajectory, different combinations of drops and media (as presented in Table I) were selected. To achieve certain drop-to-medium viscosity

TABLE I. Fluid properties of droplet.

Liquid	Interfacial tension (mNm^{-1})	Density (gcm^{-3})	Viscosity (mPa s)
Silicon oils (two different liquids)	24	0.85&1.06	10&110
Glycerol water mixture (50-50, %v)	40	1.13	8
Paraffin oil	30	0.868	122.7

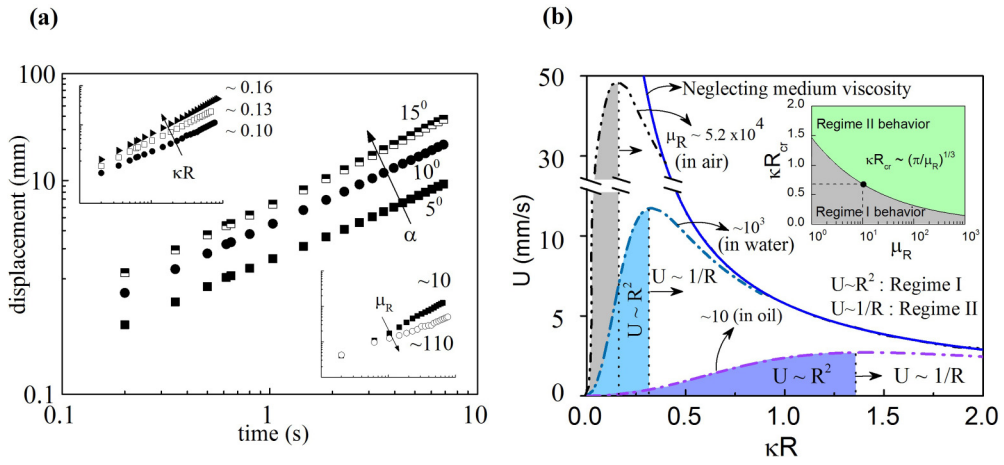

FIG. 2. (a) Droplet trajectory at different inclination angles show weak dependency of the rate of displacement (velocity) on the angle of inclination. Top-left inset shows the displacement for varying drop size κR, where $1/\kappa$ is the capillary length and R is drop radius (typically less than 1 mm). Bottom-right inset depicts the role of medium viscosity at the same inclination angle of 5°. Both the insets are presented for displacement versus time with same axes limits as figure (a). (b) Theoretical prediction for droplet velocity is plotted over nondimensional drop size κR. Mahadevan and Pomeau model [7] (solid line) ignores the medium viscosity, whereas, the present model (dashed lines) accounts for resistance from the medium. Three different cases with μ_R of the order of 10, $\sim 10^3$, and 10^4 demonstrate the role of medium viscosity. A viscous medium results in a regime (shaded region) where increase in size results in increase in the velocity. In the inset, progression of a critical or crossover length scale (κR_{cr}) towards higher drop size is observed as viscosity ratio decreases—this crossover size demarcates between the two velocity behaviors of the drop for a specific drop-to-medium viscosity ratio as shown by the dashed lines.

ratios ($\mu_R = \mu_d/\mu_m$), water (1000 kg/m^3, 1 mPa s with 0.01% Tween-20 solution), anhydrous alcohol (790 kg/m^3, 1.1 mPa s), canola oil (920 kg/m^3, 72 mPa s), and methanol (792 kg/m^3, 0.59 mPa s) were used as surrounding medium. Microscopic glass slides were used as the substrates. The combinations were selected to achieve a wide spectrum of drop-to-liquid viscosity ratios (μ_R).

To achieve a double-emulsion droplet in order to explore Regime II behavior, a coaxial needle with two different sources of liquids was used. First an outer droplet was generated inside the viscous medium and later the inner needle slowly generates another droplet inside the outer one. By inserting a denser liquid droplet into the outer drop, a double drop was achieved, which is commonly known as a double emulsion drop [20,21]. This double drop was then deposited using the needleless deposition technique. The rest of the experiments were carried out in the same way as the single phase drop experiments.

III. RESULTS AND DISCUSSION

To differentiate the sliding and rolling motions of the droplet, a marker along the periphery of the droplet (small air bubble with a drop) was introduced and the motion of this marker was tracked, as seen in Fig. 1(b). The cycloidal trajectory of the marker demonstrates the rolling mode of motion. The droplet rolls as it moves on the incline with a center of mass velocity U and in a very short time steady linear velocity is attained. In Fig. 2(a) the displacement shows a power-law dependency on time $\sim t$ as reported for glycerol drop descent (in air [4]) and metal ball descent (on an incline lubricated with a thin viscous film [14]). For a glycerol drop rolling in air medium, inverse dependency between the size of the drop and descent velocity was observed [4], whereas with a viscous medium, the dependency changes as depicted in the top-left inset of Fig. 2(a). For a liquid drop rolling in

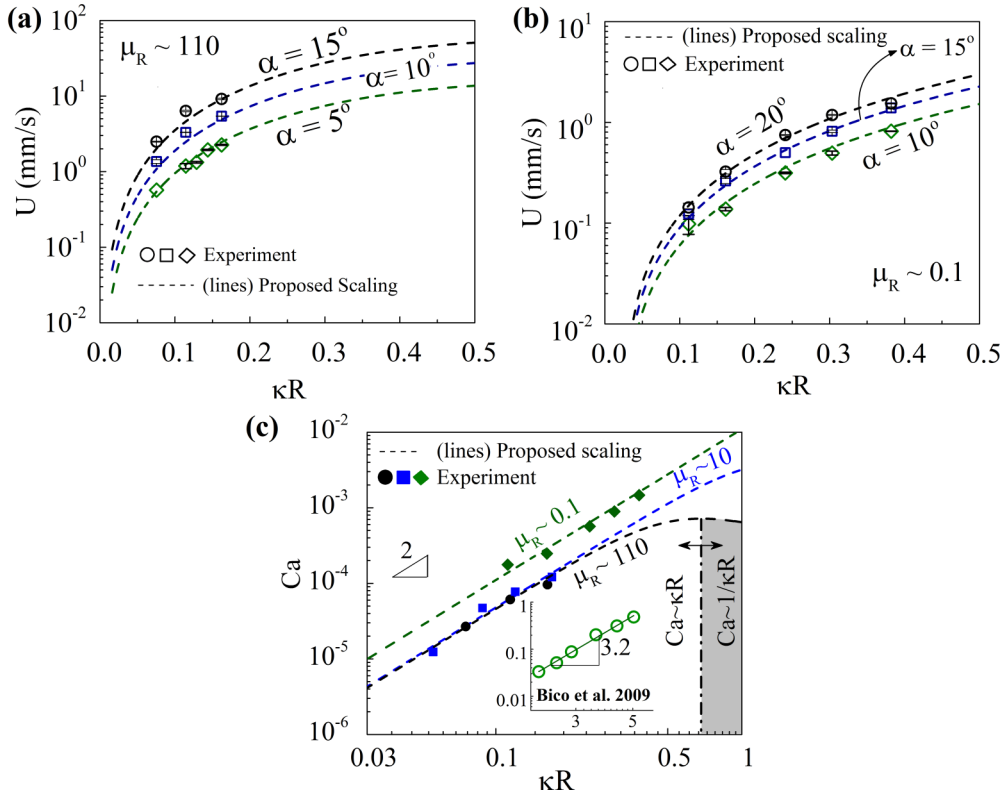

FIG. 3. Droplet motion for Regime I under different operating parameters: (a) Silicon-oil drop rolling in water medium, $\mu_R \sim 110$, at different inclination angles (open diamond—$\alpha = 5^\circ$, open rectangle—10°, and open circle—15°) (b) water-glycerol drop rolling in canola oil medium, $\mu_R \sim 0.10$, (open diamond—$\alpha = 10^\circ$, open rectangle—15°, and open circle—20°). Maximum error obtained for experiment is $\pm 8\%$. (c) Non-dimensional descent velocity of liquid droplets increases with κR in Regime I for different drop-medium combinations. Inset (reconstructed from experimental observations of Bico *et al.* (2009): [14]) shows power law dependency between the two parameters for a non-deformable body.

air, inverse dependency between size and velocity was attributed to the viscous dissipation at the contact area [4,7]. But in the presence of a viscous medium, we observed that velocity increased with increasing drop size. Further, the bottom right inset of Fig. 2(a) suggests that medium viscosity alters the magnitude of descent velocity.

In a non-wetting case, if the contact angle is close to 180°, a droplet of radius R can maintain a quasi-spherical shape forming a disk-shaped finite contact zone [7]. Most of the viscous dissipation occurs near the contact area besides that occurring within the drop. One can balance the rate of change of gravitational potential energy with viscous dissipation at the contact zone (which scales as $\sim \mu_d \frac{U^2}{R^2} \ell^3$ [7]), as well as an additional Stokes dissipation due to the presence of the surrounding viscous medium. This dissipation amounts to $\sim 6\pi \mu_m R U^2$. Here, μ_d and μ_m are drop and medium viscosity, respectively, and ℓ is the contact length that scales as $\sim \sqrt{(R\delta)}$; δ being the lowering of the center of mass of the droplet due to the slight deformation of the drop near the contact zone. These two are the major contributing forces to equilibrate the motion and the experimental results (presented in Fig. 3) suggest the same. Hence, in the presented scenario, we can justifiably ignore any rotational viscous dissipation due to the relative motion between the interfaces. Further, as the drop moves along the surface, there might be an additional resistive force near the wall, in the neighborhood of the contact area, that is different from the bulk dissipation. If this force is disregarded, the scaling

argument we present here remains unaffected and indeed predicts the obtained experimental data that will be discussed later in this article. Balancing the major contributing forces, one can obtain the following expression for drop velocity:

$$U \sim \frac{Bo\sigma \sin\alpha}{\mu_d Bo^{3/2} + 6\pi\mu_m}. \tag{1}$$

Here, σ is the interfacial tension of the drop with the considered medium and Bo is Bond number ($Bo = gR^2\Delta\rho/\sigma$). In this study, we present our results and arguments based on the characteristic length scale, $\kappa R(= Bo^{1/2})$, where $1/\kappa$ is the capillary length. A similar expression as Eq. (1), with a different pre-factor, can also be obtained by considering the dissipation in the lubrication region (the thin film region between the drop and the wall) [14,22] instead of the bulk dissipation. The asymptotic solutions of the Stokes equations for a sphere rotating with angular velocity, ω and translating velocity, U near a wall, bounding a viscous fluid with gap thickness $\epsilon(\to 0)$, give the dissipation in lubrication region as $\sim R \ln \frac{R}{\epsilon}\mu_m(U - \omega R)U$. Denoting $R \ln \frac{R}{\epsilon}$ and $(U - \omega R)U$ terms as R' and U'^2, one obtains identical scaling behavior ($\sim\mu_m R' U'^2$) as the bulk dissipation which is considered in this study.

The bulk dissipation term in Eq. (1) becomes insignificant for a medium with negligible viscosity and results in a similar expression as proposed by Mahadevan and Pomeau [7]. Considering the effect of the medium, one can express drop velocity in terms of effective viscosity (μ_{eff}) as follows:

$$U \sim \frac{\sigma \sin\alpha}{\mu_{\text{eff}} Bo^{1/2}}, \tag{2}$$

where $\mu_{\text{eff}} = \mu_d + 6\pi\mu_m/Bo^{3/2}$. A comparison between these two models (with and without considering medium viscosity) is presented in Fig. 2(b). In contrast to Mahadevan and Pomeau [7] (Regime II), emanation of another regime (Regime I)—where velocity increases with size—appears only if viscosity of the medium is considered. With these two regimes, it is evident that the velocity of a descending drop can either increase or decrease with an increase in drop size. The shaded areas of the curves in Fig. 2(b) schematically identify this Regime I where velocity increases with increasing drop size. Similar non-monotonic behavior (increasing and decreasing) for a creeping motion of non-spherical droplet sliding at a large inclination has been reported in the literature [15,16]. Hodges *et al.* [5] theoretically investigated a number of regimes of velocity behavior that depended upon slipping, sliding, or rolling mode of motion along with the shape of the liquid droplet. Their asymptotic theory for a rolling three dimensional drop suggests similar Regime I behavior. However, a distinct identification of the two regimes with experimental evidence is missing in the literature.

Figure 2(b) shows that the contrasting velocity behaviors can coexist simultaneously for a wide range of viscosity ratios. In this figure, for each case, a crossover point is observed where the corresponding droplet becomes large enough to dictate the rolling motion merely by the viscous dissipation at the contact area. The drop experiences two dissipative powers acting against its motion. Balancing these two resistive forces gives a critical/crossover length scale $(\kappa R) \sim (\pi/\mu_R)^{1/3}$ that determines the boundary between the two regimes. We will denote this limiting size as κR_{cr}. This divides the domain into two regimes which will be termed as Regime I (velocity increases with increase in size) and Regime II (velocity decreases with increase in size) in this article. Inset of Fig. 2(b) shows how the critical/crossover length scale progresses towards larger drops as viscosity ratio decreases. For example, a viscosity ratio of ~100 (as shown by the dotted lines in the plot) would results in a critical length scale of ~0.65. A drop below this dimension would travel with Regime I behavior and a larger drop would exhibit Regime II behavior. It can be noted here that for very high viscosity ratios, the critical length scale tends towards sticking thresholds [4] and for very low viscosity ratios, this length scale exceeds experimental limits.

The two regimes can be investigated for a given inclination by considering two limiting cases, i.e., negligible and comparable viscosity of the medium. When medium viscosity is negligible, μ_{eff}

becomes comparable to μ_d and $U \propto 1/Bo^{1/2}$ (i.e., $U \propto 1/R$). On the other hand, for a viscous medium the resistive components assure the coexistence of the two regimes. Theoretically, when a droplet rolls in a medium with negligible viscosity, it can experience both regimes, as shown in Fig. 2(b) by the dashed line (with $\mu_R \sim 5.2 \times 10^4$). If the drop is small enough ($<\kappa R_{cr}$), it can demonstrate Regime I behavior, i.e., $U \propto R^2$, but the realistic magnitude for a given liquid drop in air is practically impossible to achieve where the sticking threshold is difficult to surpass [4]. For example, in the case of a glycerol drop in air, this critical radius threshold results in $\sim$200 μm. Such a small drop size is almost impossible to deposit without any external kinetic energy implications. More importantly, even if a successful deposition for rolling is achieved, the contact area where the dissipation dominates the sticking threshold [4] may not permit the drop to roll [22]. These practical limitations restricted the researchers to perform experiments that can reveal the existence of Regime I. In commonly studied cases, the contact base radius increases sharply with the increase in drop size and thus invites dissipation with a greater exponent of drop size ($\propto R^4$) compared to the gravitational driving force ($\propto R^3$). Subsequently, a drop asymptotically tends to attain lower velocities as its size grows [4,7]. In Fig. 2(b), the solid line depicts the velocity variation predicted by the model presented in the literature (Regime II) [7] while the dashed lines (with $\mu_R \sim 5 \times 10^4$) represent both regimes predicted by the model presented in this study. Both models agree with each other above the crossover size (κR_{cr}) but there is disagreement below this threshold, which becomes more pronounced in the presence of a viscous medium, as demonstrated for cases using water ($\mu_R \sim 10^3$) and oil ($\mu_R \sim 10$) media.

Regime I, which is difficult to achieve in a medium with negligible viscosity (i.e., air), can easily be demonstrated by altering the medium viscosity. In viscous medium, smaller droplet size results in point contact as opposed to the finite contact length during the droplet descent. This makes the dissipation at the contact area almost negligible compared to the gravitational driving force and bulk dissipation from the surrounding medium. The displaced center of gravity [by an amount δ, as shown in Fig. 1(b)] of the rolling droplet, due to its own weight, becomes significantly above κR_{cr} where all three forces have same order of magnitude and hence transition to Regime II can be noticed. Since the contact length ℓ scales as $\sim\sqrt{R\delta}$, the contact area can be regarded as a point contact for drops with size less than κR_{cr}. Increasing the medium viscosity dominance (or decrease drop to medium viscosity ratio), Regime I operating zone can be maneuvered. As observed in Fig. 2(b), if medium viscosity is magnified by two orders, the operating range for drop size in Regime I widens significantly. However, the experimental domain is constricted by several factors. Besides the sticking thresholds and creeping flow assumptions, the needleless deposition technique imposes further limitations in selecting the liquid combinations. Additionally, the necessity of immiscibility and inert nature between the drop and medium is paramount. With these restrictions in mind, the combinations of drop and medium liquids are selected for investigating Regime I in a detailed manner.

In Figs. 3(a) and 3(b), steady state drop velocities for viscosity ratios $\sim$110 and $\sim$0.1 are presented against κR at different inclinations. The dashed lines are the velocity predictions by Eq. (1) and symbols represent the corresponding experimental outcome. To account for the geometric constants in the scaling analysis, an appropriate empirical coefficient has been added to the theoretical prediction as a multiplying factor, i.e., $U_{\text{exp}} = k \times U_{th}$ (where $k = \pi/3$). One can normalize the velocity as Capillary number ($Ca = \mu U/\sigma$) where viscosity can be of either the medium or the drop. To pinpoint the importance of the medium viscosity, Ca in Fig. 3(c) is defined with medium viscosity. Our results show excellent qualitative agreement with the proposed scaling analysis and therefore we suggest that our experiment allowed us to explore regime I for the rolling drop motion. For $\mu_R \sim 110$, as drop size increases by a factor of $\sim$1.5 (κR from 0.05 to 0.08), velocity increases by a factor of $\sim$4. A further increase in drop size by the same factor ($\sim$1.5) results in merely $\sim$2.9 times increment in velocity. Thus velocity experiences a diminishing increment as drop size increases and will reach a maximum magnitude at κR_{cr}, prior to beginning to exhibit Regime II behavior.

In Regime I, the deformation of the contact area and hence the associated dissipation can be ignored. It allows us to observe an increasing trend that is compatible with intuitions for a rigid

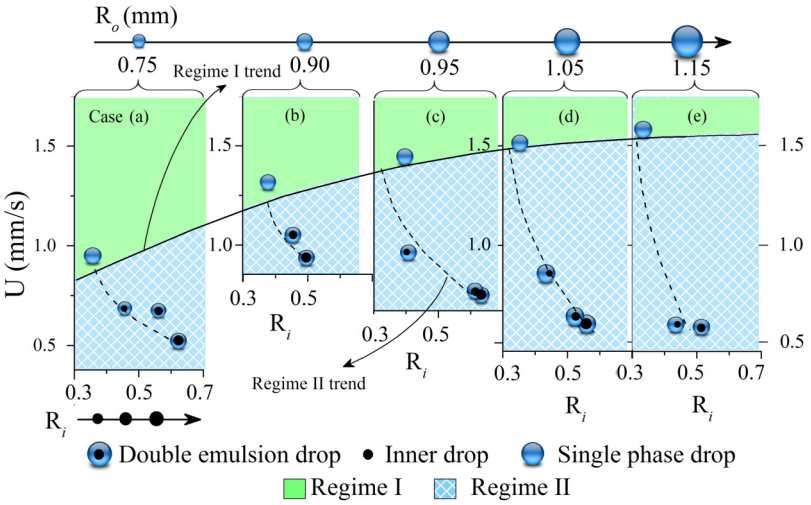

FIG. 4. Occurrence of both regimes for drop descent with double-emulsion drop on a 3° incline. The increment in velocity with increase in size [regime I of Fig. 2(b)] is obtained by increasing the overall size of the drop. Increment in the droplet size is presented on the top x axis. As presented in the hatched areas of Cases (a)–(e), Regime II behavior (decrements in the velocity) is observed with an increment in the dissipation by inserting an inner drop for a fixed outer drop size. Symbols are experimental results while the dashed and solid lines denote the velocity trend observed from the experimental data.

body. This reminds us of the work of Bico *et al.* [14], where motion of a rolling sphere on an incline lubricated with a thin viscous film is studied. The motion of the rigid body [14] exhibits a stronger power-law dependency (3.2 ± 0.05), as seen in the inset of Fig. 3(c). The difference in the power-law between the two cases (deformable drop and rigid body descent) is another aspect that we would like to bring to the reader's attention. The presence of an outer viscous medium along the entire interface of the drop, as opposed to thin film at the contact area, may be the cause of the nonconformity of the exponents. However, the present soft body study being very different from the rigid-body motion, this comparison is tentative only.

In order to extend our analysis of liquid drops to witness Regime II behavior in a viscous medium, κR needs to be significantly larger. For example, with $\mu_r \sim 100$, κR should be $\geqslant 0.65$, which results in a drop diameter of ~ 5 mm. Achieving a drop of this radius is restricted by the spherical shape assumption. In this case, to retain a spherical shape, a drop radius must be smaller than ~ 1.9 mm; larger drops undergo too much deformation. For a highly viscous medium (i.e., $\mu_R \sim 0.1$) this size is too big to attain. On the other hand in a medium with low viscosity (i.e., $\mu_R \sim 10^4$), the drop size is too small to avoid the sticking threshold. These limitations impede us from performing the experimental analysis with the considered combinations of drop and medium. Therefore, we have carefully engineered the experiments to overcome this barrier so that we might still observe Regime II. If κR of the drop can be increased above κR_{cr} without altering the drop size (so that its spherical shape is not deformed), exploration of Regime II becomes easier. The apparent dilemma between size and deformation can be easily solved by instilling a denser and immiscible liquid drop inside the rolling drop. This allows us to observe the rolling of a double emulsion drop consisting of both inner and outer drop phases. This not only facilitates the demonstration of the contrasting velocity behaviors, it also widens the degree of freedom for the selection of liquids for experimentation.

We introduced denser inner droplets of varied radii into the outer drops in such a way that the overall drop radius remained constant. We have termed the set of experiments with one fixed drop radius as one 'case' in Fig. 4. Thus cases (a)–(e) in Fig. 4 denote five different sets of experiments where the inner drop size is altered, maintaining a fixed overall double drop size for each particular

case. For a fixed double drop size, introducing a denser inner drop increases κR of the droplet without altering the shape and the overall drop size. Thus the Stokes outer bulk dissipation remains the same for each case but the increment of κR causes further dissipation. For a constant overall drop size, the dominant dissipation, at the contact area, results in the decrease in velocity with increase in κR, as commonly observed. The dashed lines connecting the experimental velocity in Fig. 4 highlight Regime II, while the solid line shows the increasing trend (Regime I) of the velocity. It is worth considering the role of the newly introduced interface between the outer and inner drop. Relative motion between the inner and outer drop along this interface might invite an additional internal dissipation in addition to the dissipation that occurs in the vicinity of the contact area. As discussed earlier, the viscous dissipation near the contact area scales as the fourth exponent of the characteristic radius; similarly, the additional viscous dissipation due to the relative motion at the new interface, may also scale with the same exponent of the characteristic length scale, such that it may scale as $\sim Ri^4$. It is plausible that this dissipation also accounts for the decrements in velocity as the area of the interface is increased with increasing inner drop radius. The rationale for scaling argument for this dissipation is from the understanding of viscous dissipation near the contact area of drop. Exact quantification of this dissipation requires further investigations in detail.

IV. CONCLUSION

A liquid droplet rolling down an incline in a viscous medium attains higher velocities as its size increases up to a critical length scale. Above this length scale, velocity decreases with increasing drop size. Thus two distinct behaviors of drop rolling motion can be identified in the presence of an outer viscous medium. Drop and medium viscosity significantly dictate the critical length restriction and the boundary between these two regimes. By altering the viscous dissipation at the contact area without sacrificing the size restriction, non-intuitive decrements in drop velocity can be witnessed.

ACKNOWLEDGMENTS

The authors thank Natural Sciences and Engineering Research Council (NSERC) for the financial support in the form of Grant No. RGPIN-2015- 06542. We also thank the reviewers for their insightful comments that led to an improvement of this work. Our sincere gratitude extends to Prof. Howard A. Stone for providing us with additional comments in bringing further clarity to the article.

[1] J. A. Schwartz, J. V. Vykoukal, and P. R. C. Gascoyne, Droplet-based chemistry on a programmable micro-chip, Lab Chip **4**, 11 (2004).
[2] G. Katsikis, J. S. Cybulski, and M. Prakash, Synchronous universal droplet logic and control, Nat. Phys. **11**, 588 (2015).
[3] D. R. Link, E. Grasland-Mongrain, A. Duri, F. Sarrazin, Z. Cheng, G. Cristobal, M. Marquez, and D. A. Weitz, Electric control of droplets in microfluidic devices, Angew. Chem., Int. Ed. **45**, 2556 (2006).
[4] D. Richard and D. Quéré, Viscous drops rolling on a tilted non-wettable solid, Europhys. Lett. **48**, 286 (1999).
[5] S. Hodges, O. Jensen, and J. Rallison, Sliding, slipping and rolling: The sedimentation of a viscous drop down a gently inclined plane, J. Fluid Mech. **512**, 95 (2004).
[6] L. Gao and T. J. McCarthy, Contact angle hysteresis explained, Langmuir **22**, 6234 (2006).
[7] L. Mahadevan and Y. Pomeau, Rolling droplets, Phys. Fluids **11**, 2449 (1999).
[8] P. Aussillous and D. Quéré, Liquid marbles, Nature **411**, 924 (2001).
[9] G. G. Stokes, On the effect of the internal friction of fluids on the motion of pendulums, Trans. Cambridge Philos. Soc. **9**, 8 (1851).
[10] H. Allen, L. The motion of a sphere in a viscous fluid, Philos. Mag. Ser. 5 **50**, 519 (1900).

[11] L. Rayleigh, On the motion of solid bodies through viscous liquid, Philos. Mag. Ser. 6 **21**, 697 (1911).
[12] P. G. Saffman, The lift on a small sphere in a slow shear flow, J. Fluid Mech. **22**, 385 (1965).
[13] A. N. Prokunin, On a paradox in the motion of a rigid particle along a wall in a fluid, Fluid Dyn. **38**, 443 (2003).
[14] J. Bico, J. Ashmore-Chakrabarty, G. McKinley, and H. Stone, Rolling stones: The motion of a sphere down an inclined plane coated with a thin liquid film, Phys. Fluids **21**, 082103 (2009).
[15] A. J. Griggs, A. Z. Zinchenko, and R. H. Davis, Gravity-driven motion of a deformable drop or bubble near an inclined plane at low Reynolds number, Int. J. Multiphase Flow **34**, 408 (2008).
[16] A. J. Griggs, A. Z. Zinchenko, and R. H. Davis, Creeping motion and pending breakup of drops and bubbles near an inclined wall, Phys. Fluids **21**, 093303 (2009).
[17] P. R. Waghmare, S. Das, and S. K. Mitra, Drop deposition on under-liquid low energy surfaces, Soft Matter **9**, 7437 (2013).
[18] P. R. Waghmare and S. K. Mitra, Needle-free drop deposition technique for contact angle measurements of superhydrophobic surfaces, J. Appl. Phys. **116**, 114903 (2014).
[19] P. R. Waghmare, S. Mitra, N. S. K. Gunda, and S. K. Mitra, Needle-free drop deposition: the role of elastic membranes, RSC Advances **5**, 82374 (2015).
[20] A. S. Utada, E. Lorenceau, D. R. Link, P. D. Kaplan, H. A. Stone, and D. A. Weitz, Monodisperse double emulsions generated from a microcapillary device, Science **308**, 537 (2005).
[21] S.-H. Kim, J. W. Kim, J.-C. Cho, and D. A. Weitz, Double-emulsion drops with ultra-thin shells for capsule templates, Lab Chip **11**, 3162 (2011).
[22] K.-Y. Law and H. Zhao, *Surface Wetting: Characterization, Contact angle, and Fundamentals* (Springer, Berlin, 2015).